

## Network Numerical Simulation of Impulsively-Started Transient Radiation-Convection Heat and Mass Transfer in a Saturated Darcy-Forchheimer Porous Medium

O. Anwar Bég<sup>1,2</sup>, J. Zuco<sup>3</sup>, H. S. Takhar<sup>4</sup>, T. A. Bég<sup>5</sup>

<sup>1</sup>Aerodynamics Program, BAE Systems, Apartment G09D, Salwa Garden Village  
PO Box 1732, Riyadh, 11441, Kingdom of Saudi Arabia

<sup>2</sup>Engovation Engineering Science Research  
15 Southmere Avenue, Bradford, BD7 3NU, England, UK  
docoanwarbeg@hotmail.co.uk

<sup>3</sup>Thermal Engineering and Fluids Department  
ETS Ingenieros Industriales Campus Muralla del Mar  
Universidad Politécnica de Cartagena, 30203 Cartagena (Murcia), Spain  
joaquin.zuoco@upct.es

<sup>4</sup>Engineering Department, Manchester Metropolitan University  
Manchester, M5 1GD, England, UK  
h.s.takhar@mmu.ac.uk

<sup>5</sup>18 Milton Grove, Manchester, M16 0BP, England, UK

**Received:** 24.10.2007    **Published online:** 28.08.2008

**Abstract.** We study the effects of thermal radiation and porous drag forces on the natural convection heat and mass transfer of a viscous, incompressible, gray, absorbing-emitting fluid flowing past an impulsively started moving vertical plate adjacent to a non-Darcian porous regime. The governing boundary-layer equations are formulated in an  $(X^*, Y^*, t^*)$  coordinate system with appropriate boundary conditions. The Rosseland diffusion approximation is employed to analyze the radiative heat flux and is appropriate for non-scattering media. The model is non-dimensionalized and solved with the network simulation model. We study the influence of Prandtl number, radiation-conduction parameter, thermal Grashof number, species Grashof number, Schmidt number, Darcy number and Forchheimer number on the dimensionless velocity, temperature and species function distributions. Additionally we compute the variation of the local skin friction, Nusselt number and Sherwood number for selected thermophysical parameters. Increasing Darcy number is seen to accelerate the flow; the converse is apparent for an increase in Forchheimer number. Thermal radiation is seen to reduce both velocity and temperature in the boundary layer. The interactive effects of second order porous drag and thermal radiation are also considered. The model finds applications in solar energy collection systems, porous combustors, transport in fires in porous media (forest fires) and also the design of high temperature chemical process systems.

**Keywords:** thermal radiative heat transfer, Rosseland model, convection, mass transfer, non-Darcian regime, network numerical simulation, energy systems, Nusselt and Sherwood number.

## 1 Introduction

Many high temperature processes in industrial design and combustion and fire science involve thermal radiation heat transfer in combination with conduction, convection and also mass transfer. For example radiative-convective heat transfer flows arise in industrial furnace systems [1], astrophysical flows [2], forest fire dynamics [3], fire spread in buildings [4] etc. Considerable research has therefore appeared studying radiative-convective flows in a variety of geometrical configurations with numerical and mathematical models. Bratis and Novotny [5] reported on the effects of thermal radiation in the convection boundary layer-regime of an enclosure. Chang et al. [6] used a radiative flux diffusion approximation to model the interaction of convective and radiative heat transfer in two-dimensional complex enclosure. Hossain et al. [7] studied the effects of thermal radiation heat transfer on combined forced and free convection boundary layer flow past a horizontal cylinder. Chamkha [8] studied numerically the combined influence of radiative flux, gravity field and heat absorption on convection heat transfer in a two-phase flow. Hossain and Vafai [9] reported on the natural convection boundary layer heat transfer with variable viscosity, suction and radiation effects. Chamkha et al. [10] studied computationally the influence of mass transfer and radiation flux on natural convection flows. More recently Pop et al. [11] considered the radiative-convective stagnation flow over a stretching surface. These analyses were however confined to regimes where there is only a fluid present. Extensive applications exist however where the medium is porous medium. For example in environmental and geothermal energy systems, convection and radiation heat transfer take place in porous geomaterials. Forest fire spread also constitutes an important application of radiative-convective heat transfer, as described by Meroney [12]. More recently Chittrphiromsri and Kuznetsov [13] have studied the influence of high-intensity radiation in unsteady thermofluid transport in porous wet fabrics as a model of firefighter protective clothing under intensive flash fires. Their computational study showed that moisture in the fabric begins to vaporize initially from the outer surface of the fabric to the inner surface during heating, with a component of the moisture recondensing in the interior during cooldown. Temperature distributions in the fabric layers were shown to be strongly affected by moisture content and thermal radiation flux. Generally for low velocity hydromechanics of porous media, a Darcian model is used which relates the bulk matrix impedance in the regime to the pressure drop. This approach is generally accurate for situations where Reynolds number is less than approximately 10. Beyond this value inertial effects become significant and must be incorporated in mathematical models. Both Darcian and Darcy-Forchheimer (inertial) models have been employed extensively in radiative-convection flows in porous media. Chamkha [14] studied the influence of solar radiation on free convection in an isotropic, homogenous porous medium using a computational method. Mohammadein et al. [15] employed a regular two-parameter perturbation analysis in studying the radiative flux effect on free convection in a non-Darcian porous medium. They studied four different flow regimes i.e. that adjacent to the isothermal surface, flow with a uniform heat flux, plane plume flow and also

the flow generated from a horizontal line energy source on a vertical adiabatic surface. Radiation was found to significantly affect all flow cases. Takhar et al. [16] used an implicit difference scheme and the Cogley-Vincenti-Giles non-gray model to simulate the radiation-convection gas flow in a non-Darcy porous medium with viscous heating effects. Radiation parameter was found to strongly affect temperature distributions. Satapathy et al. [17] studied the natural convection heat transfer in a Darcian porous regime with Rosseland radiative flux effects. El-Hakiem et al. [18] considered the radiation-convection flow in a non-Darcy porous medium numerically. Nagaraju et al. [19] used the Schuster-Schwartzchild two-flux radiative model and the Blottner finite difference scheme to investigate the combined radiative and convective heat transfer in a medium with variable porosity. Takhar et al. [20] employed a Runge-Kutta-Merson shooting quadrature and the Rosseland diffusion algebraic radiation model to analyze the mixed radiation-convection flow in a non-Darcy porous medium, showing that temperature gradients are boosted with radiative flux. More recently Chamkha et al. studied [21] the influence of thermal radiation on steady natural convection in a viscoelastic-fluid saturated non-Darcian porous medium using the Keller Box numerical scheme. Temperatures were seen to be substantially boosted with an increase in radiative parameter. Other studies discussing the effects of radiation on convection flows in porous media have been communicated by Raptis and Perdakis [22] who considered transient flows and Takhar et al. [23]. In certain industrial systems, the flow past an impulsively started plate is also important. Such flows are transient and therefore temporal velocity and temperature gradients have to be included in the analysis. Excellent work in this regard has been presented by Stewartson [24] although his study ignored heat transfer. Later Soundalgekar [25] extended this study obtaining Laplace transform solutions for the natural convection and mass transfer effects on flow past an impulsively-started vertical surface. More recently Muthukumaraswamy and Ganesan [26] considered the transient heat and mass transfer past an impulsively-started vertical plate. Impulsive flows with thermal radiation effects and in porous media are also important in chemical engineering systems, aerodynamic blowing processes and geophysical energy modeling. Raptis and Singh [27] studied numerically the natural convection boundary layer flow past an impulsively started vertical plate in a Darcian porous medium. More recently Ganesan et al. [28] have studied the influence of thermal radiation on convection flows past an impulsively started plate. Thusfar however the transient laminar heat and mass transfer past an impulsively-started surface embedded in a non-Darcian porous medium with thermal radiation present has to the authors' knowledge not been considered. We shall therefore study this problem numerically in the present paper. Such a study has significant applications in solar collection systems, fire dynamics in insulations, and also geothermal energy systems. The transformed problem is shown to be dictated by eight thermophysical parameters, viz dimensionless time, thermal Grashof number, species Grashof number, Darcy number, Reynolds number, Forchheimer number, Prandtl number and Schmidt number. The influence of these parameters on the velocity profiles, temperature function, mass transfer function, local shear stress, local Nusselt number and local Sherwood number are presented and discussed at length.

## 2 Mathematical model

We study the laminar unsteady viscous free convection heat and species transfer of an incompressible, absorbing, emitting and non-scattering, gray, Newtonian fluid past an impulsively started vertical semi-infinite surface adjacent to an isotropic, non-Darcian, porous medium. The physical model is shown in Fig. 1.

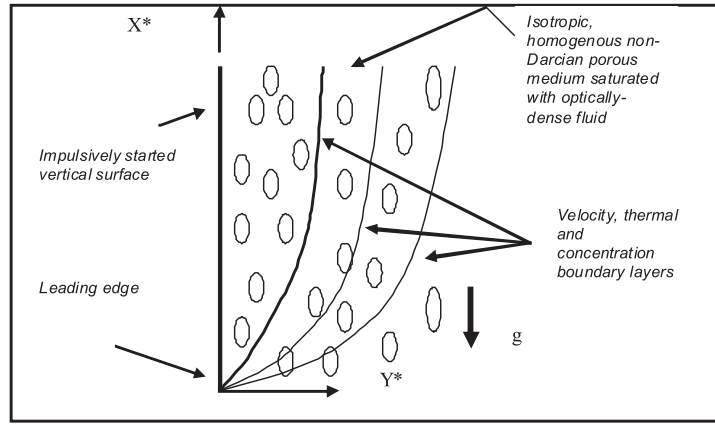


Fig. 1. Physical model and coordinate system.

The  $X^*$  direction is located parallel to the plate surface and the  $Y^*$  direction normal to it. The plate and fluid are taken to be at the same temperature. The concentration of species diffusing in the binary mixture is much lower than the concentration of chemical species otherwise present. We neglect stratification, anisotropic porous and viscous heating effects in our analysis. At time  $t^* = 0$ , the plate commences impulsive motion in the  $X^*$  direction, with constant velocity  $u_0^*$ , and the plate temperature and concentration levels are instantaneously elevated. These new values are sustained for all time  $t^* > 0$ . Thermal radiation is assumed to be present in the form of a unidirectional flux in the  $Y^*$  direction i.e.  $q_r$  (transverse to the vertical surface). The Rosseland diffusion flux model is used and is defined following Modest [1] as follows:

$$q_r = -\frac{4\sigma}{3\kappa'} \frac{\partial T^{*4}}{\partial Y^*}. \quad (1)$$

Under the Boussinesq approximation, the boundary layer equations for mass, momentum, energy and species conservation in an  $(X^*, Y^*)$  coordinate system, can be shown to take the form:

*Mass conservation*

$$\frac{\partial U^*}{\partial X^*} + \frac{\partial V^*}{\partial Y^*} = 0; \quad (2)$$

*Momentum conservation*

$$\begin{aligned} \frac{\partial U^*}{\partial t^*} + U^* \frac{\partial U^*}{\partial X^*} + V^* \frac{\partial U^*}{\partial Y^*} = g\beta[T^* - T_\infty^*] + g\beta^*[C^* - C_\infty^*] \\ + \nu \frac{\partial^2 U^*}{\partial Y^{*2}} - \frac{\nu}{K}U - \frac{b}{K}U^2; \end{aligned} \quad (3)$$

*Energy (heat) conservation*

$$\frac{\partial T^*}{\partial t^*} + U^* \frac{\partial T^*}{\partial X^*} + V^* \frac{\partial T^*}{\partial Y^*} = \alpha \frac{\partial^2 T^*}{\partial Y^{*2}} - \frac{1}{\rho C_p} \frac{\partial q_r}{\partial Y^*}; \quad (4)$$

*Species conservation*

$$\frac{\partial C^*}{\partial t^*} + U^* \frac{\partial C^*}{\partial X^*} + V^* \frac{\partial C^*}{\partial Y^*} = D \frac{\partial^2 C^*}{\partial Y^{*2}}. \quad (5)$$

The corresponding temporal and spatial boundary conditions are prescribed as:

$$t^* \leq 0: \quad U^* = 0, \quad V^* = 0, \quad T^* = T_\infty^*, \quad C^* = C_\infty^*, \quad (6)$$

$$t^* > 0: \quad U^* = U_0^*, \quad V^* = 0, \quad T_w^* = T_\infty^*, \quad C^* = C_\infty^* \quad \text{at } Y^* = 0, \quad (7)$$

$$U^* = 0, \quad T^* = T_\infty^*, \quad C^* = C_\infty^* \quad \text{at } X^* = 0, \quad (8)$$

$$U^* \rightarrow 0, \quad T^* \rightarrow T_\infty^*, \quad C^* \rightarrow C_\infty^* \quad \text{as } Y^* \rightarrow \infty, \quad (9)$$

where  $X^*$  and  $Y^*$  are coordinates,  $U^*$ ,  $V^*$  are velocity components in the  $X^*$ ,  $Y^*$  directions,  $t^*$  is dimensionless time,  $\sigma$  is the Stefan-Boltzmann constant,  $g$  is gravitational acceleration,  $\kappa'$  is the mean absorption coefficient,  $\beta$  is coefficient of thermal expansion,  $\beta^*$  is mass transfer coefficient of expansion,  $\nu$  is the kinematic viscosity of the gray fluid,  $T^*$  is temperature,  $C^*$  is species concentration,  $K$  is the permeability (hydraulic conductivity of the porous medium with dimensions  $m^2$ ),  $b$  is the Forchheimer geometrical inertia parameter of the porous medium,  $\alpha$  is the thermal diffusivity,  $D$  is the species diffusivity,  $(\ )_w$  denotes conditions at the wall (vertical surface) and  $(\ )_\infty$  designates conditions in the free stream (outside the boundary layers). Following Raptis and Perdakis [22] we can express the quartic temperature function in (1) as a *linear* function of temperature. The Taylor series for  $T^{*4}$ , discarding higher order terms can be shown to give:

$$T^{*4} \sim 4T_\infty^{*3} - 3T_\infty^{*4}. \quad (10)$$

Substitution of this expression into (1) and then the heat conservation equation (4), eventually leads to the following form of the energy equation:

$$\frac{\partial T^*}{\partial t^*} + U^* \frac{\partial T^*}{\partial X^*} + V^* \frac{\partial T^*}{\partial Y^*} = \alpha \frac{\partial^2 T^*}{\partial Y^{*2}} + \frac{16\sigma T_\infty^{*3}}{3\kappa' \rho C_p} \frac{\partial^2 T^*}{\partial Y^{*2}}. \quad (11)$$

Equations (2), (3), (5) and (11) with boundary conditions (6) to (9) constitute a two-point boundary value problem which is fairly challenging to solve. We therefore non-dimensionalize the model to facilitate a numerical solution by the *network model*. This serves to introduce standard thermofluid parameters such as the Prandtl number etc and also allows general solutions relevant to any size of the flow regime.

### 3 Transformation of model

Defining:

$$\begin{aligned}
 X &= \frac{X^*U_0^*}{\nu}, & Y &= \frac{Y^*U_0^*}{\nu}, & U &= \frac{U^*}{U_0^*}, & V &= \frac{V^*}{U_0^*}, \\
 t &= \frac{t^*U_0^{*2}}{\nu}, & T &= \frac{T^* - T_\infty^*}{T_w^* - T_\infty^*}, & C &= \frac{C^* - C_\infty^*}{C_w^* - C_\infty^*}, \\
 Pr &= \frac{\nu}{\alpha}, & Sc &= \frac{\nu}{D}, & Da &= \frac{K}{L^2}, & Fs &= \frac{b}{L}, & Re &= \frac{U_0^*L}{\nu}, & N &= \frac{\kappa'k}{4\sigma T_\infty^{*3}}, \\
 Gr &= \frac{g\beta\nu(T_w^* - T_\infty^*)}{U_0^{*3}}, & Gm &= \frac{g\beta^*\nu(C_w^* - C_\infty^*)}{U_0^{*3}},
 \end{aligned} \tag{12}$$

where  $X$  and  $Y$  are dimensionless coordinates,  $U$  and  $V$  dimensionless velocities,  $t$  is dimensionless time,  $T$  is dimensionless temperature function,  $C$  is dimensionless concentration function,  $N$  is the conduction-radiation heat transfer parameter,  $Pr$  is Prandtl number,  $Sc$  is Schmidt number,  $Da$  is Darcy number,  $Fs$  is the Forchheimer inertial number,  $Re$  is the Reynolds number,  $Gr$  is thermal Grashof number and  $Gm$  is species Grashof number. Introducing these transformations into equations (2), (3), (5) and (11) we arrive at the following dimensionless conservation equations:

$$\frac{\partial U}{\partial X} + \frac{\partial V}{\partial Y} = 0, \tag{13}$$

$$\frac{\partial U}{\partial t} + U \frac{\partial U}{\partial X} + V \frac{\partial U}{\partial Y} = GrT + GmC + \frac{\partial^2 U}{\partial Y^2} - \left[ \frac{1}{DaRe^2} \right] U - \left[ \frac{Fs}{DaRe} \right] U^2, \tag{14}$$

$$\frac{\partial T}{\partial t} + U \frac{\partial T}{\partial X} + V \frac{\partial T}{\partial Y} = \frac{1}{Pr} \left[ 1 + \frac{4}{3N} \right] \frac{\partial^2 T}{\partial Y^2}, \tag{15}$$

$$\frac{\partial C}{\partial t} + U \frac{\partial C}{\partial X} + V \frac{\partial C}{\partial Y} = \frac{1}{Sc} \frac{\partial^2 C}{\partial Y^2}. \tag{16}$$

The corresponding initial and end boundary conditions now take the form:

$$t \leq 0: \quad U = 0, \quad V = 0, \quad T = 0, \quad C = 0, \tag{17}$$

$$t > 0: \quad U = 1, \quad V = 0, \quad T = 1, \quad C = 1 \quad \text{at } Y = 0, \tag{18}$$

$$U = 0, \quad T = 0, \quad C = 0 \quad \text{at } X = 0, \tag{19}$$

$$U \rightarrow 0, \quad T \rightarrow 0, \quad C \rightarrow 0 \quad \text{as } Y \rightarrow \infty. \tag{20}$$

The following quantities are also of interest for thermal design in for example energy systems engineering, namely the local skin friction, local Nusselt number and the local Sherwood number. They provide a good estimate of the basic heat and mass transfer processes in the flow regime. Following Incropera and Dewitt [29] these functions are

computed with the following mathematical expressions:

$$\tau_X = - \left[ \frac{\partial U}{\partial Y} \right]_{Y=0}, \quad (21)$$

$$Nu_X = -X \left[ \frac{\partial T}{\partial Y} \right]_{Y=0}, \quad (22)$$

$$Sh_X = X \left[ \frac{\partial C}{\partial Y} \right]_{Y=0}, \quad (23)$$

where the appropriate value for the streamwise coordinate,  $X$ , can be utilized. Additionally mean values of these parameters can be defined as follows:

$$\bar{\tau} = - \int_0^1 \left[ \frac{\partial U}{\partial Y} \right]_{Y=0} dX, \quad (24)$$

$$\bar{Nu} = - \int_0^1 \left[ \frac{\partial T}{\partial Y} \right]_{Y=0} dX, \quad (25)$$

$$\bar{Sh} = - \int_0^1 \left[ \frac{\partial C}{\partial Y} \right]_{Y=0} dX. \quad (26)$$

#### 4 Special cases of the model

A number of special cases can be derived from the transformed momentum, energy and species conservation equations in order to test the accuracy of the numerical method employed in this study:

##### Case 1. Transient radiative free convective heat and mass transfer in a gray fluid-saturated Darcian porous medium

For the case where  $Fs \rightarrow 0$ , the inertial porous drag effects vanish and the momentum equation (14) reduces to:

$$\frac{\partial U}{\partial t} + U \frac{\partial U}{\partial X} + V \frac{\partial U}{\partial Y} = GrT + GmC + \frac{\partial^2 U}{\partial Y^2} - \left[ \frac{1}{DaRe^2} \right] U. \quad (27)$$

The other transport equations remain unaffected as do the boundary conditions.

##### Case 2. Transient radiative free convective heat and mass transfer in a gray fluid medium

With  $Da \rightarrow \infty$ , all porous hydrodynamical body forces vanish. This implies that the porous matrix permeability becomes infinite so that the regime is purely fluid. Again we can modify the momentum equation (27) to the reduced form:

$$\frac{\partial U}{\partial t} + U \frac{\partial U}{\partial X} + V \frac{\partial U}{\partial Y} = GrT + GmC + \frac{\partial^2 U}{\partial Y^2}. \quad (28)$$

This version of the momentum equation was studied by Prasad et al. [30].

### Case 3. Transient free convective heat and mass transfer in a non-Darcian porous medium without radiation

As  $N \rightarrow \infty$ , thermal radiation heat flux effects vanish in the limit. The regime is therefore only *purely free convection heat and mass transfer*. In this case only the energy equation (15) now reduces from:

$$\frac{\partial T}{\partial t} + U \frac{\partial T}{\partial X} + V \frac{\partial T}{\partial Y} = \frac{1}{Pr} \frac{\partial^2 T}{\partial Y^2}. \quad (29)$$

The other transport equations remain unchanged from (13), (14) and (16).

### Case 4. Transient radiative forced convective heat and mass transfer in a non-Darcian porous medium

When  $Gr \rightarrow 0$  and  $Gm \rightarrow 0$ , the buoyancy effects vanish and the temperature and concentration fields become de-coupled from the momentum equation. Only the momentum equation is affected which reduces from the general case, (14) to:

$$\frac{\partial U}{\partial t} + U \frac{\partial U}{\partial X} + V \frac{\partial U}{\partial Y} = \frac{\partial^2 U}{\partial Y^2} - \left[ \frac{1}{DaRe^2} \right] U - \left[ \frac{Fs}{DaRe} \right] U^2. \quad (30)$$

## 5 Numerical solution by network simulation method

Numerical solutions to the governing transformed equations (13) to (16) under boundary conditions (17) to (20) are to be obtained using the network simulation method. This method has been used efficiently by Zueco and co-workers [31–33] and is now briefly described. The starting point for this method is always the discretization of the equations that form the mathematical model of the problem under study, (13) to (16). This discretization is based on the finite-difference formulation, and only a discretization of the spatial co-ordinates is necessary, while time remains as a real continuous variable, thereby transforming the partial differential equations into a set of ordinary differential equations (ODEs) which can then be described by an *elemental network cell*. Unlike the usual numerical methods, in the NSM the independent variable reticulation is successive since we carry out first the spatial and then the temporal reticulation to solve the circuit equations. This difference in the reticulation may provide us with some advantages in the use of the NSM, at least in certain problems. No time interval needs to be established by the users to obtain the numerical solution, the time interval sets automatically in every iteration according to the given stability and convergence requirements, and this means without a doubt an advantage. A second advantage is that with the NSM we must only transform PDEs into ODEs and the latter along with the initial and boundary conditions must be formulated in terms of circuit. The program to solve ODEs is based on the network model. In other methods algorithms are rather more complex and require considerable programming efforts. For the transient analysis, Pspice uses the numerical

implicit integration formulae (trapezoidal integration) with an order two accuracy; additionally a central-difference methodology has been used for the approximation of first and second spatial-derivatives. As a result second order accuracy of the spatial discretization is achieved. Based on the governing discretized equations, an electrical network circuit is design for each equation, where these equations are formally equivalent to the discretized equations. The finite-difference differential equations resulting from dimensionless continuity, momentum balance, energy balance and mass balance equations (13)–(16) are:

$$\begin{aligned} \Delta Y \frac{dU_{i,j}}{dt} + U_{i,j}(U_{i+\Delta X,j} - U_{i-\Delta X,j})\Delta Y/\Delta X + V_{i,j}(U_{i,j+\Delta Y} - U_{i,j-\Delta Y}) \\ = \Delta Y Gr T_{i,j} + \Delta Y Gm C_{i,j} + (U_{i,j-\Delta Y} - U_{i,j})/(\Delta Y/2) \\ - (U_{i,j} - U_{i,j+\Delta Y})/(\Delta Y/2) - \Delta Y U_{i,j}(Re + FsU_{i,j})/(DaRe), \end{aligned} \quad (31)$$

$$\begin{aligned} \Delta Y Pr \frac{dT_{i,j}}{dt} + U_{i,j}(T_{i+\Delta X,j} - T_{i-\Delta X,j})\Delta Y/\Delta X + Pr V_{i,j}(T_{i,j+\Delta Y} - T_{i,j-\Delta Y}) \\ = (T_{i,j-\Delta Y} - T_{i,j})[2(1 + 4/3N^{-1})]/\Delta Y \\ - (T_{i,j} - T_{i,j+\Delta Y})[2(1 + 4/3N^{-1})]/\Delta Y, \end{aligned} \quad (32)$$

$$\begin{aligned} \Delta Y Sc \frac{dC_{i,j}}{dt} + \Delta Y Sc U_{i,j}(C_{i+\Delta X,j} - C_{i-\Delta X,j})/\Delta X + Sc V_{i,j}(C_{i,j+\Delta Y} - C_{i,j-\Delta Y}) \\ = (C_{i,j-\Delta Y} - C_{i,j})/(\Delta Y/2) - (C_{i,j} - C_{i,j+\Delta Y})/(\Delta Y/2). \end{aligned} \quad (33)$$

The terms that contains these equations can be treated as electrical currents, due that the electric-(motion-thermal-mass) analogy and the current Kirchhoff's law are considered (Zueco [34]). This analogy can be applied is such away that the variables velocity ( $U, V$ ), temperature ( $T$ ) and concentration ( $C$ ) are equivalent to the variable, voltage, while the velocity flux ( $\partial U/\partial X, \partial U/\partial Y$ ), heat flux ( $\partial T/\partial X, \partial T/\partial Y$ ) and concentration flux ( $\partial C/\partial X, \partial C/\partial Y$ ) are equivalent to the variable, electric current. NSM simulates the behaviour of unsteady electric circuits by means of resistors, capacitors and non-linear devices that seek to resemble thermal systems governed by unsteady linear or non-linear equations. Another noticeable advantage of the NSM is that it provides both the velocity and velocity flux density fields immediately (without no need of numerical manipulation). Later, an electrical network circuit is designs to model the boundary conditions. The whole network must be converted into a suitable program that is solved by a computer code in a PC using suitable software, Pspice [35] in this work. A mesh system with  $20 \times 200$  nodes is proven to suggest mesh-independent results. An advantage of the NSM is that the derivatives involved in equations (21) to (23) are directly evaluated, while other methods for example using five-point approximation formula. The integrals (24) to (26) are evaluated using Newton-Cotes closed integration formula.

To test the accuracy of the NSM simulations we have compared the transient velocity profiles versus  $Y$  at  $X = 1.0$  and the steady-state local skin friction distributions versus axial coordinate,  $X$ , for various combinations of  $Gr$ ,  $Gm$ ,  $Sc$  and  $N$  with the Crank-Nicolson central difference computations of Prasad et al. [30]. The comparisons are shown in Figs. 2 and 3 and found to be in excellent agreement.

Extensive computations have been performed for the effects of the controlling thermo-fluid and hydrodynamic parameters on dimensionless velocities ( $U, V$ ), temperature

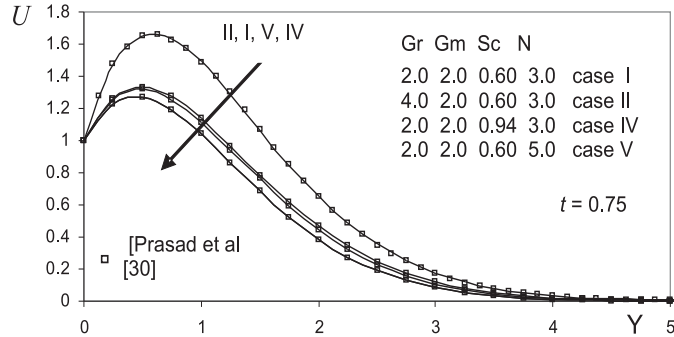


Fig. 2. Transient velocity profiles at  $X = 1.0$  for various  $Gr$ ,  $Gm$ ,  $Sc$  and  $N$  values.

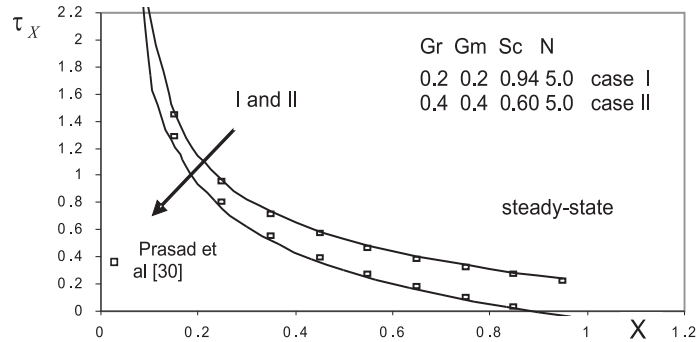


Fig. 3. Steady state local skin friction profiles versus  $X$  for various  $Gr$ ,  $Gm$ ,  $Sc$  and  $N$  values.

( $T$ ) and concentration ( $C$ ), and also on the local skin friction ( $\tau_x$ ), local Nusselt number ( $Nu_x$ ) and local Sherwood number ( $Sh_x$ ). In addition we have aimed to study the interactional effects of for example Forchheimer drag ( $F_s$ ) and thermal radiation parameter ( $N$ ). Only selective figures have been reproduced here for brevity. Default values of the parameters are as follows: conduction-radiation parameter ( $N$ ) i.e. Stark number  $N = 0.5$ , Forchheimer parameter  $F_s = 0.1$ , thermal Grashof number  $Gr = 1$ , species Grashof number  $Gm = 1$ , Prandtl number  $Pr = 0.7$  (air), Darcy number  $Da = 0.1$ , Schmidt number  $Sc = 0.5$  (water vapour) and Reynolds number  $Re$  of unity. All graphs therefore correspond to these values unless specifically indicated on the appropriate graph. We have also opted to study the spatial variation of variables at a certain time e.g. for  $t = 1$ . Separate transient profiles have also been computed. The present analysis concerns the case of optically thick boundary layers, where the thermal boundary layer is expected to become very thick as the medium is highly absorbing. The radiative diffusion (Rosseland model) adds a radiative conductivity to the conventional thermal conductivity. The effect of radiation is to thicken the thermal boundary layer

similar to the effect of decreasing Prandtl number (the latter representing the ratio of the viscous to thermal diffusion). Radiation supplements the thermal diffusion effectively enhancing the thermal diffusivity, as described by Siegel and Howell [36].

Figs. 4 to 8 illustrate the effects of  $N$ ,  $Da$ ,  $Gr$ ,  $Gm$ ,  $Pr$  respectively on the dimensionless temperature profiles versus  $Y$  (transverse coordinate) at  $t = 1$ . An increase in  $N$  corresponds to an increase in the relative contribution of conduction heat transfer to thermal radiation heat transfer. As  $N \rightarrow \infty$ , conduction heat transfer dominates and the contribution of thermal radiative flux vanishes. The converse is true for  $N = 0$  where thermal radiation dominates over conduction [20]. Small values of  $N$  therefore physically correspond to stronger thermal radiation flux and in accordance with this, the maximum temperatures are observed in Fig. 4 for  $N = 0.1$ . As  $N$  increases to 0.5, 1, 3, 5 and 100, considerable reduction is observed in the temperature values,  $T$ , from the peak value at the wall ( $Y = 0$ ) across the boundary layer regime to the free stream where  $Y = 10$ , at

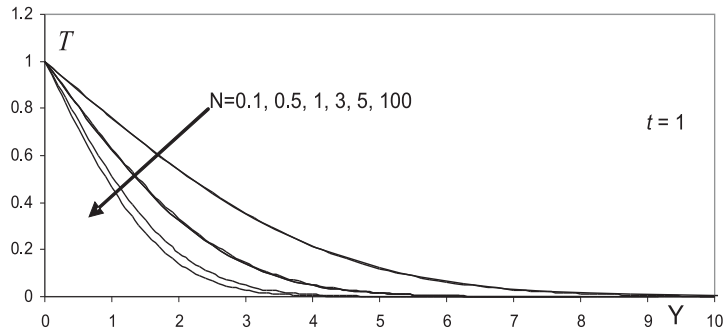


Fig. 4. Transient temperature distribution with  $Y$  for various conduction-radiation parameters ( $N$ ).

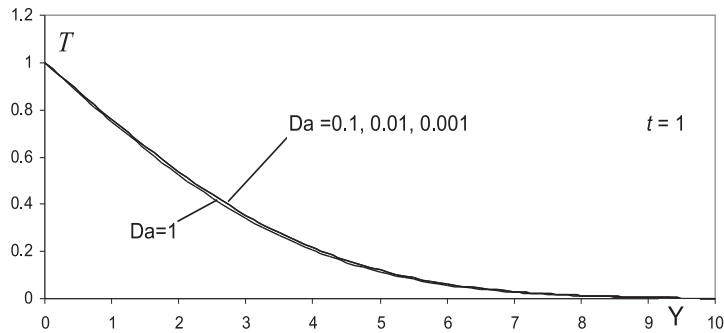


Fig. 5. Transient temperature distribution with  $Y$  for various Darcy numbers ( $Da$ ).

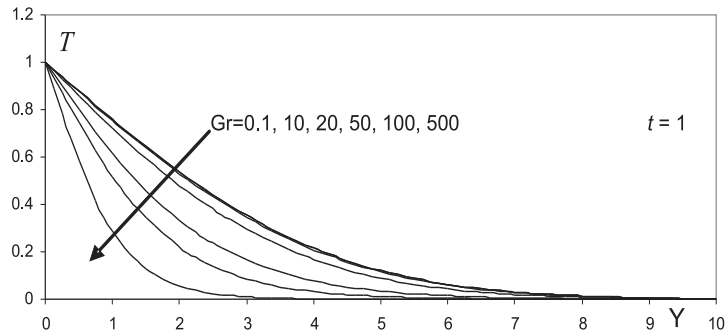


Fig. 6. Transient temperature distribution with  $Y$  for various thermal Grashof numbers ( $Gr$ ).

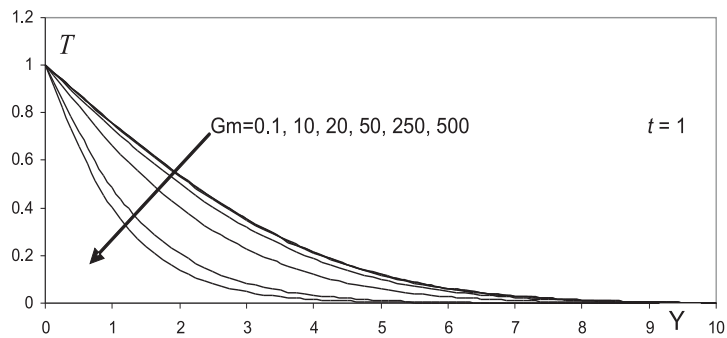


Fig. 7. Transient temperature distribution with  $Y$  for various species Grashof number ( $Gm$ ).

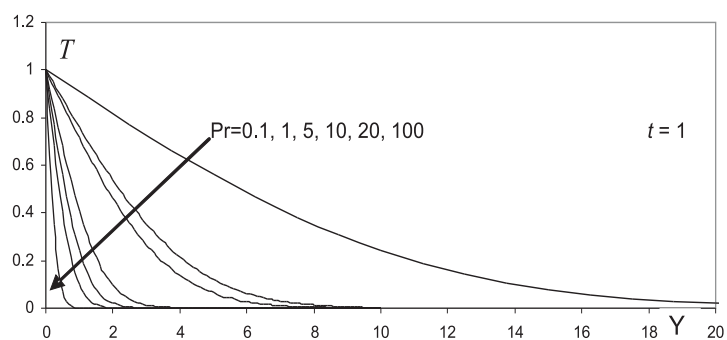


Fig. 8. Transient temperature distribution with  $Y$  for various Prandtl numbers ( $Pr$ ).

which point temperatures are negligible for any value of  $N$ . All profiles decay asymptotically to zero in the free stream. We also observe that the relative decrease in temperature from  $N = 0.1$  to  $0.5$  is greatest; separation of profiles reduces from  $N = 0.5$  to  $1$  (almost identical) and progressively so to  $N = 5$  and  $N = 10$ . In Fig. 5 a small decrease in temperature accompanies a tenfold rise in  $Da$  from  $0.1$  to  $1$ ; the effect of a rise in  $Da$  (implying an increase in permeability and a simultaneous decrease in Darcian drag force) implies that conduction heat transfer becomes less prominent than convection heat transfer (there is less solid material present in the porous medium) and this contributes to the marginal decrease in temperatures across the boundary layer from the wall to the free stream. The influence of thermal Grashof number,  $Gr$  on temperatures is shown in Fig. 6.  $Gr$  signifies the relative effect of the thermal buoyancy force to the viscous hydrodynamic force in the boundary layer regime. An increase in  $Gr$  from  $0.1$  through  $20$ ,  $30$ ,  $50$ ,  $200$  and  $500$  induces a sizeable decrease in the temperature throughout the porous regime. The temperature distributions descend smoothly from their maxima of unity at the wall ( $Y = 0$ ) to zero at the edge of the boundary layer. Thermal buoyancy therefore depresses temperatures in the medium. A similar trend is observed for the species Grashof number,  $Gm$ , as shown in Fig. 7. Again temperatures are seen to fall with a rise in  $Gm$  from  $0.1$  to  $500$ ; however the profiles descend less steeply than for  $Gr$  i.e. there is a more gradual reduction in temperatures. The influence of Prandtl number ( $Pr$ ) on  $T$  profiles with  $Y$  coordinate is shown in Fig. 8.  $Pr$  defines the ratio of momentum diffusivity to thermal diffusivity i.e. it controls the thickness of the thermal boundary layer and the rate of heat transfer. For  $Pr = 1$ , the momentum and thermal boundary layer thicknesses, as described by Schlichting [37], are approximately of equal extent. For fluids possessing a large viscosity (high  $Pr$  fluids e.g. oils), the ability to transport momentum is large. As a result the elimination of momentum introduced by the presence of the boundary (no slip condition of Prandtl at the wall), extends considerably into the fluid causing the velocity boundary layer to be relatively large. We therefore expect that with an increase in  $Pr$  the thermal boundary layer will be decreased in thickness and there will be a corresponding uniformity of temperature distributions across the boundary layer. The profiles in Fig. 8 attest to this where we observe that the maximum temperatures correspond to lowest  $Pr$  values ( $0.1$ ), and progressively decrease as  $Pr$  rises. The profiles also steepen and intersect the abscissa faster for higher  $Pr$  fluids i.e. temperatures across the boundary layer (normal to the wall) reach zero faster for higher  $Pr$  fluids. The lower  $Pr$  values may correspond to certain metallic fluids while  $Pr$  of  $1$  corresponds to approximately water. Higher  $Pr$  values ( $100$ ) are observed in high viscosity working fluids, oils, lubricants etc.

Figs. 9 to 12 depict the effects of  $N$ ,  $Da$ ,  $Fs$  and  $Sc$  on temperature profiles versus  $X$ , for constant  $Y$  and  $t$  values i.e. there are snapshots in time and at a fixed location from the wall. Fig. 9 shows the effect of conduction-radiation parameter,  $N$  (i.e. Stark number) on the temperature variation along the vertical surface i.e. in the streamwise direction, at  $t = 1$ ,  $Y = 1.25$  i.e. at some small distance into the boundary layer regime, a short time after impulsive loading has been initiated. Although we have computed the time taken to reach the steady-state for various  $N$  values, and it has been found that, as with the finite difference calculations of Prasad et al. [30], the equilibration time is increased with an increase in  $N$ , this has not been reproduced here for brevity. Our computations

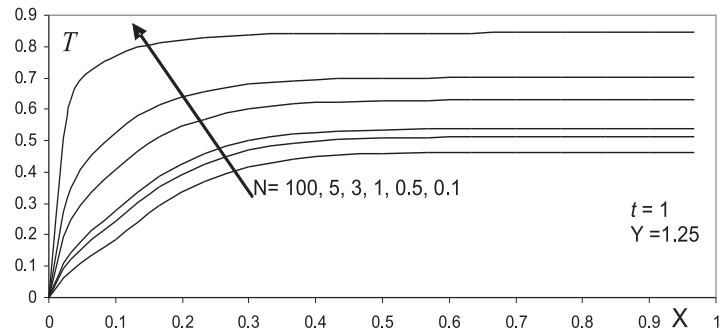


Fig. 9. Transient temperature distribution with  $X$  for various conduction-radiation numbers ( $N$ ) at  $Y = 1.25$ .

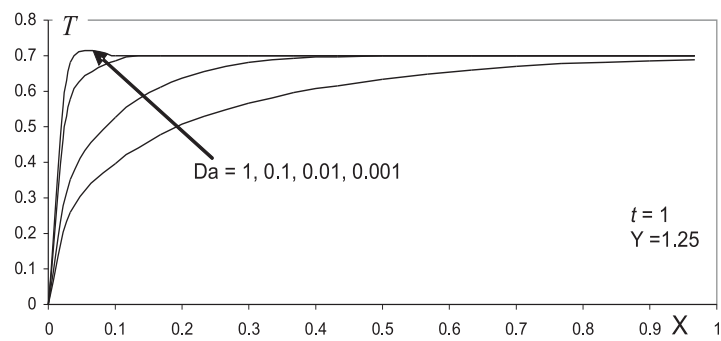


Fig. 10. Transient temperature distribution with  $X$  for various Darcy numbers ( $Da$ ) at  $Y = 1.25$ .

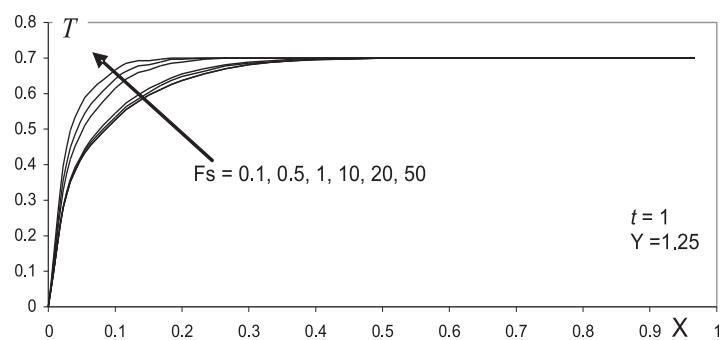


Fig. 11. Transient temperature distribution with  $X$  for various Forchheimer numbers ( $Fs$ ) at  $Y = 1.25$ .

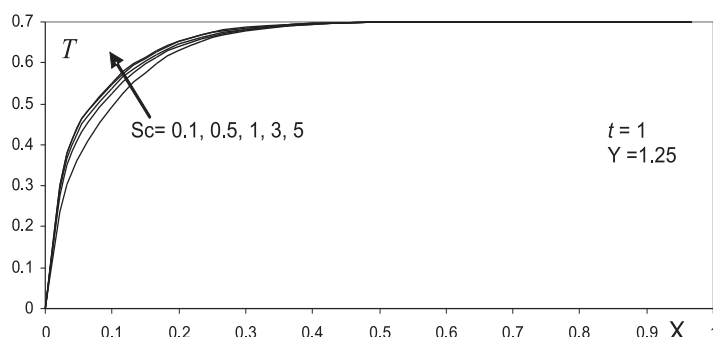


Fig. 12. Transient temperature distribution with  $X$  for various Schmidt numbers ( $Sc$ ) at  $Y = 1.25$ .

indicate that as  $N$  decreases from 100 (low radiation contribution) through 5, 3, 1, 0.5 and to 0.1 (strong radiation), the temperatures are increased markedly throughout the length of the wall i.e. along the  $X$  direction. The values in all cases are higher than for the  $Y$ -variation due to the proximity of the regime to the wall, from which the radiative flux emanates. As a result in both distributions the thermal boundary layer thickness is decreasing due to a rise in  $N$  values i.e. it increases with a decrease in  $N$ . The effect of the Darcy number on  $T$  versus  $X$  profiles is shown in Fig. 10. As observed for the  $T$  versus  $Y$  profiles, again an increase in permeability ( $Da$  value) causes a decrease in temperatures along the wall direction. Maximum temperatures correspond therefore to the lowest  $Da$  value (0.001 i.e. very low permeability implying high solid material presence and strong conduction heat transfer contribution, especially near the leading edge i.e.  $X \sim 0.05$ ); the lowest temperatures are observed for  $Da = 1$  (for which the Darcian drag force is a minimized for this graph), for which the profile is approximately monotonic and more evenly dispersed throughout the  $X$  domain. Fig. 11 shows the effect of the second order porous drag parameter i.e.  $Fs$  on  $T$  versus  $X$  distributions. Conversely to  $Da$  effects, a rise in  $Fs$  (implying greater inertial drag force contribution) causes a rise in temperature values. The influence of the Schmidt number,  $Sc$ , on  $T$  versus  $X$  profiles is shown in Fig. 12.  $Sc$  embodies the ratio of the momentum diffusivity to the mass (species) diffusivity. Larger  $Sc$  fluids will therefore have lower mass diffusion properties i.e. concentration boundary layers will be thinner than the velocity (hydrodynamic) boundary layer thickness. This is analogous to higher  $Pr$  fluids for which the thermal boundary layer will be much thinner than the velocity boundary layer [37]. A rise in  $Sc$  from 0.1 through 0.5, 1, 3 and to 5 induces a rise in temperatures. Profiles are in all cases monotonic although they become steeper for higher  $Sc$  values.  $Sc$  of 0.5 approximately represents water and  $Sc$  of 1 approximates well to that for Carbon Dioxide. Higher values are associated with hydrocarbon working fluids. For example  $Sc = 2$  would represent Ethyl Benzene. The increase in  $T$  with  $Sc$  has been computed also by Prasad [30], however they only considered the distribution transverse to the wall i.e. in the  $Y$  direction for constant  $X$  ( $X = 1.0$ ). The importance of our numerical calculations may be exploited in

for example controlling temperatures in energy systems, using lower viscosity fluids i.e. lower  $Sc$  fluids.

Figs. 13 to 15 represent the distribution of streamwise velocity,  $U$ , with streamwise distance,  $X$ , at fixed  $t$  and  $Y$  values, for the effects of  $F_s$ ,  $N$  and  $Da$  respectively. As expected, an decrease in  $F_s$  induces a substantial increase in transient velocity,  $U$ . In the momentum equation (14), the quadratic drag term,  $-\left[\frac{F_s}{DaRe}\right]U^2$  is directly proportional to  $F_s$ . Consequently as  $F_s$  increases from 0.1, through 0.5, 1, 10, 20 to 50, we observe a dramatic fall in  $U$  velocity component which is sustained shortly downstream from the leading edge ( $X \sim 0.05$ ) throughout the wall length up to  $X = 1.0$ . Fig. 14 shows the distribution of  $U$  against  $X$  for various  $N$  values. As with temperatures, a decrease in radiation contribution (corresponding to a rise in  $N$  value) causes a large decrease in transient velocity,  $U$ . Our results concur with those obtained by Prasad [30]. Fig. 15 reveals that a rise in Darcy number (from 0.01, through 0.1, 0.3, 0.5 to 1) accompanying a decrease in Darcian porous resistance in the momentum equation (14) i.e.  $-\left[\frac{1}{DaRe^2}\right]U$ ,

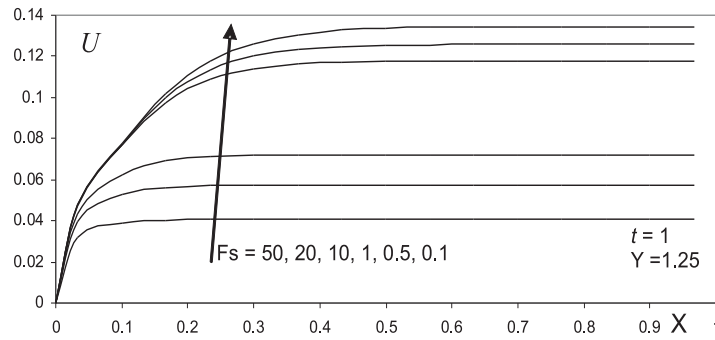


Fig. 13. Transient velocity distribution with  $X$  for various Forchheimer numbers ( $F_s$ ) at  $t = 1$  and  $Y = 1.25$ .

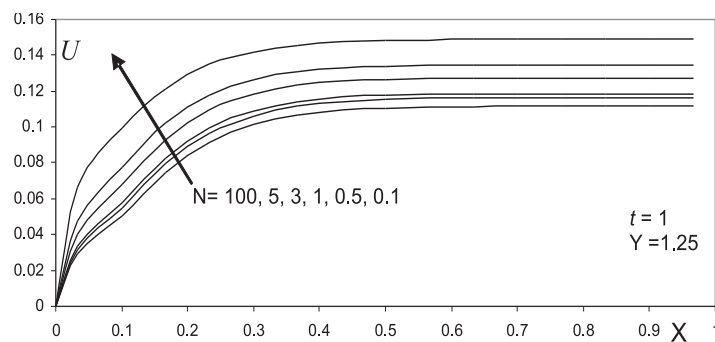


Fig. 14. Transient velocity distribution with  $X$  for various conduction-radiation numbers ( $N$ ) at  $t = 1$  and  $Y = 1.25$ .

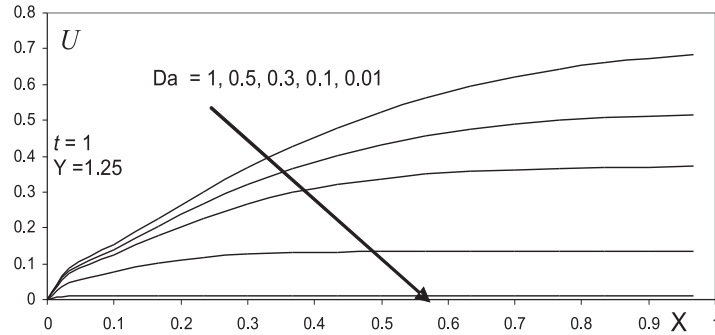


Fig. 15. Transient velocity distribution with  $X$  for various Darcy numbers ( $Da$ ) at  $t = 1$  and  $Y = 1.25$ .

induces a substantial rise in transient velocity,  $U$ . Higher permeability regimes offer less fiber resistance to the flow and therefore it is accelerated compared with lower permeability (i.e. lower  $Da$ ) regimes which offer more resistance to the flow causing a deceleration i.e. reduction in velocity,  $U$ . This trend is maintained along the plate length i.e. for  $0 < X < 1$ .

Figs. 16 and 17 show the influence of thermal Grashof number ( $Gr$ ) and Stark conduction-radiation number ( $N$ ) on the spanwise variation in transient concentration ( $C$ ) and streamwise variation in transient concentration ( $C$ ), respectively. A rise in  $Gr$  from 0.1 to 500 (Fig. 16) causes a strong decrease in species concentration throughout the boundary layer regime from  $Y = 0$  (at the wall) to  $Y = 6.0$ . Profiles decrease asymptotically from a maximum at the wall to zero in the free stream.  $Gr$  is therefore a useful control parameter i.e. buoyancy can be used to regulate the species concentration distributions. This may be of importance in for example near and far field migration of heat-generating waste materials in underground geo-repositories. An increase in

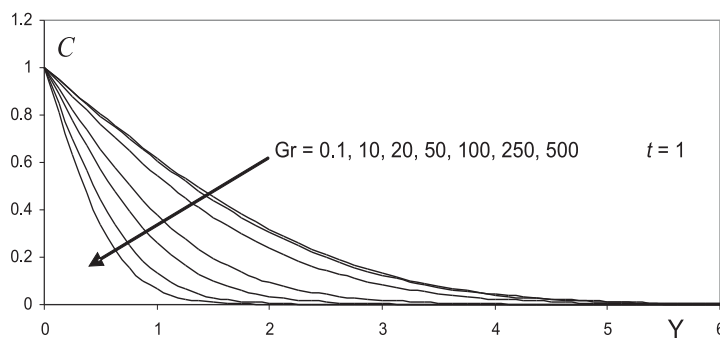


Fig. 16. Transient concentration distribution with  $Y$  for various thermal Grashof numbers ( $Gr$ ) at  $t = 1$ .

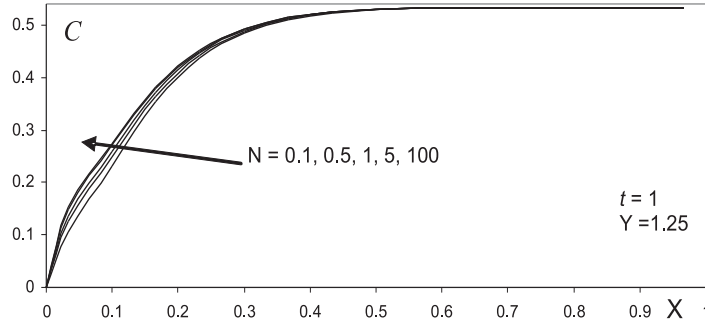


Fig. 17. Transient concentration distribution with  $X$  for various conduction-radiation numbers ( $N$ ) at  $t = 1$  and  $Y = 1.25$ .

conduction-radiation parameter ( $N$ ) (Fig. 17) is seen to decrease slightly the concentration profiles. Thermal radiation indirectly affects the diffusion conservation equation (16) via the coupling of the momentum equation to the former (in the term  $GmC$ ) and the coupling of the latter to the energy conservation equation (15) via the thermal buoyancy term,  $GrT$ . As a result there is weak effect of thermal radiation experienced by the concentration field, explaining the less dramatic influence of  $N$  on  $C$  profiles compared with Fig. 16.

Finally using expressions (21) to (23) we have computed in Figs. 18 to 20, the variation of transient local skin friction, local Nusselt number and local Sherwood number with streamwise distance for the selected effects of  $N$ ,  $Da$  and  $Fs$  parameter, at fixed time,  $t = 1$ .

Shear stress,  $\tau_X$ , at the wall ( $Y = 0$ ), as shown in Fig. 18, is illustrated for combinations of  $N$  and  $Fs$ . For Darcian flow,  $Fs = 0$ , which corresponds to Case 1 (discussed earlier), we observe that the shear stress values,  $\tau_X$ , are noticeably above those for  $Fs = 0.1$  for all values of Stark number ( $N$ ) i.e. shear stress at the wall is increased with a decrease in  $Fs$ . For purely Darcian convection, the flow will be accelerated compared with weakly Darcy-Forchheimer convection ( $Fs = 0.1$ ) for which it will be slightly decelerated. Increasing  $N$  (i.e. decreasing radiation contribution) also causes a slight increase in wall shear stress, which is understandable due to the indirect effect of radiation flux on the momentum equation (14) via the thermal buoyancy coupling with the energy conservation equation (15). The local Nusselt number,  $Nu_X$ , is seen to be increased with a rise in  $Da$  (and  $Fs$ ) as seen in Fig. 19. Hence with higher permeability media, wall heat transfer rate is enhanced since the regime becomes increasingly fluid with a rise in  $Da$  allowing a dominance of thermal convection over conduction, the latter being more significant in lower  $Da$  regimes. This behaviour is maintained throughout the wall length i.e. for all  $X$ . We note that there is a minute difference in  $Nu_X$  profiles for  $Fs = 0.1$  compared with the purely Darcian case. Values are slightly higher with non-zero  $Fs$  owing to the increase in thermal convection and heat transfer rate from the wall caused by the deceleration induced by Forchheimer effects (however small). A similar

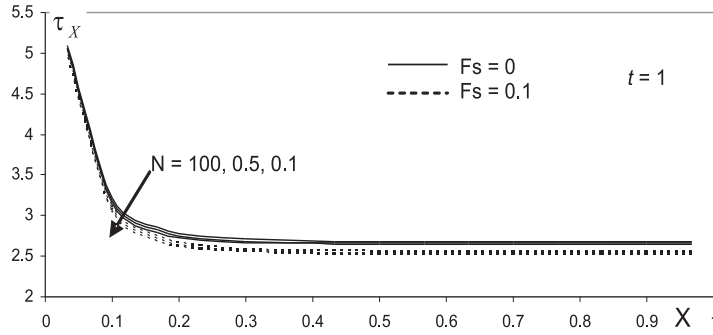


Fig. 18. Transient local skin friction distribution with  $X$  for various conduction-radiation numbers ( $N$ ) and Forchheimer numbers ( $F_s$ ) at  $t = 1$  and  $Y = 0$ .

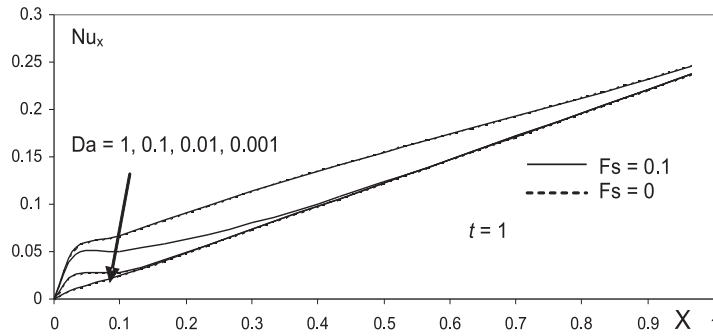


Fig. 19. Local Nusselt number distribution with  $X$  for various Darcy numbers ( $Da$ ) and Forchheimer numbers ( $F_s$ ) at  $t = 1$  and  $Y = 0$ .

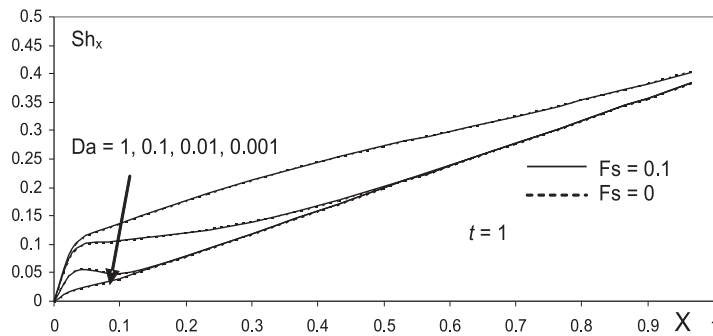


Fig. 20. Local Sherwood Number with  $X$  for various Darcy numbers ( $Da$ ) and Forchheimer numbers ( $F_s$ ) at  $t = 1$  and  $Y = 0$ .

trend is observed for the  $Sh_X$  profiles versus  $X$  with  $Da$  and  $Fs$  values (Fig. 20).  $Sh_X$  is maximized at higher  $Da$  values i.e. greater species diffusion rate from the wall to the fluid takes place for more porous regimes. Such a feature may be exploited in chemical reactor systems and energy systems where higher diffusion rates from the wall to the working fluid are required.

## 6 Conclusions

A mathematical model has been presented for the radiative-convective flow in a gray absorbing-emitting fluid-saturated porous medium adjacent to a vertical impulsively started surface. The Rosseland diffusion flux model has been used to simulate radiative flux. A Darcy-Forchheimer porous medium drag force model is utilized with isotropic permeability. The Network Simulation Method has been used to compute the dimensionless velocity, and concentration profiles. Several important special cases of the flow regime are described. We have studied graphically the influence of the effects of conduction-radiation parameter ( $N$ ), Forchheimer parameter ( $Fs$ ), thermal Grashof number ( $Gr$ ), species Grashof number ( $Gm$ ), Prandtl number ( $Pr$ ), Darcy number ( $Da$ ), Schmidt number and also time on the pertinent dependent variables. It has been shown that:

1. Increasing  $N$ ,  $Da$ ,  $Gr$ ,  $Gm$  and  $Pr$  reduces temperature,  $T$ , whereas a rise in  $Fs$  and  $Sc$  increases temperatures along the wall and transverse to the wall.
2. A decrease in  $Fs$  induces a substantial increase in transient velocity,  $U$ .
3. A decrease in radiation contribution (corresponding to a rise in  $N$  value) causes a large reduction in transient velocity,  $U$ .
4. A rise in Darcy number induces a substantial rise in transient velocity,  $U$ .
5. A rise in  $Gr$  induces a considerable decrease in species concentration,  $C$ .
6. An increase in conduction-radiation parameter ( $N$ ) causes a small decrease in concentration,  $C$ .
7. Shear stress  $\tau_X$ , at the wall is increased with a decrease in  $Fs$ .
8. Local Nusselt number,  $Nu_X$ , is increased with a rise in  $Da$  (and  $Fs$ )
9.  $Sh_X$  is increased with a rise in  $Da$  values.

The present model is currently being extended to more complex radiative transfer models e.g. Schuster-Schwartzchild two-flux model. The results of these investigations will be communicated in the future.

## Acknowledgements

Dr. O. A. Bégin would like to express his gratitude to his parents and his wife, Khush, for their excellent support with his work. The support of Leeds College of Building, during March 2007 (when the mathematical model in this work was developed) is gratefully acknowledged, in particular the gracious support of Miss Janet Jakubovic. A special thankyou to Mr. Malcolm Firth CIOB, Huddersfield Technical College, UK, for his much-appreciated support and positive attitude to engineering research.

## References

1. M. F. Modest, *Radiation Heat Transfer*, MacGraw-Hill, New York, 1993.
2. M. H. Mansour, Radiative and free convection effects on the oscillatory flow past a vertical plate, *Astrophysics Space Science J.*, **166**, pp. 26–45, 1990.
3. F. A. Albin, *Program BURNUP: A simulation model of the burning of large woody natural fuels*, Final Report, Research Grant INT-92754-GR, USFS to Montana State University (Mechanical Engineering Department), 1994.
4. R. O. Weber, Analytical model for fire spread due to radiation, *Combustion and Flame J.*, **78**, pp. 398–408, 1989.
5. J. C. Bratis, J. R. Novotny, Radiation-convection interaction in the boundary layer-regime of an enclosure, *Int. J. Heat Mass Transfer*, **17**, pp. 365–379, 1974.
6. C. Chang, K. T. Kang, J. R. Lloyd, Radiation-natural convection interaction in two-dimensional complex enclosure, *ASME J. Heat Transfer*, **105**, pp. 89–95, 1983.
7. M. A. Hossain, M. Kutibuddin, H. S. Takhar, Radiation interaction on combined forced and free convection across a horizontal cylinder, *Int. J. Applied Mechanics and Engineering*, **4**, pp. 219–235, 1999.
8. A. J. Chamkha, Effects of heat absorption and thermal radiation on heat transfer in a fluid-particle flow past a surface in the presence of a gravity field, *Int. J. Thermal Sciences*, **39**, pp. 605–615, 2000.
9. K. K. Hossain, K. Vafai, The effect of radiation on free convection flow of fluid with variable viscosity from a porous vertical plate, *Int. J. Thermal Sciences*, **40**, pp. 115–124, 2001.
10. A. J. Chamkha, H. S. Takhar, V. M. Soundalgekar, Radiation effects on free convection flow past a semi-infinite vertical plate with mass transfer, *Chemical Engineering Journal*, **84**, pp. 335–342, 2001.
11. S. R. Pop, T. Grosan, I. Pop, Radiation effects on the flow near the stagnation point of a stretching sheet, *Technische Mechanik*, **25**, pp. 100–106, 2005.
12. R. N. Meroney, *Fires in Porous Media: Natural and Urban Canopies*, NATO Advanced Study Institute, Flow and Transport Processes in Complex Obstructed Geometries: From Cities and Vegetative Canopies to Industrial Problems, May 5–15, Kiev, Ukraine, 2004.

13. P. Chitrphirimsri, A.V. Kuznetsov, Porous medium model for investigating transient heat and moisture transport in firefighter protective clothing under high intensity thermal exposure, *J. Porous Media*, **8**(5), pp. 10–26, 2005.
14. A. J. Chamkha, Solar radiation assisted natural convection in a uniform porous medium supported by a vertical flat plate, *ASME Journal of Heat Transfer*, **119**, pp. 89–96, 1997.
15. A. A. Mohammadein, M. A. Mansour, S. M. El Gaied, R. S. R. Gorla, Radiative effect on natural convection flows in porous media, *Transport Porous Media*, **32**(3), pp. 263–283, 1998.
16. H. S. Takhar, O. A. Bég, M. Kumari, Computational analysis of coupled radiation-convection dissipative non-gray gas flow in a non-Darcy porous medium using the Keller-Box implicit difference scheme, *Int. J. Energy Research*, **22**, pp. 141–159, 1998.
17. S. Satapathy, A. Bedford, S. Bless, A. Raptis, Radiation and free convection flow through a porous medium, *Int. Comm. Heat Mass Transfer*, **25**(2), pp. 289–297, 1998.
18. M. A. El-Hakiem, R. S. R. Gorla, Radiative effects in non-Darcy axisymmetric free convection in a porous medium, *Int. J. Applied Mechanics Engineering*, **5**(4), pp. 913–921, 2000.
19. P. Nagaraju, A. J. Chamkha, H. S. Takhar, B. C. Chandrasekhara, Simultaneous radiative and convective heat transfer in a variable porosity medium, *Heat and Mass Transfer J.*, **37**, pp. 243–250, 2001.
20. H. S. Takhar, O. A. Bég, A. J. Chamkha, D. Filip, I. Pop, mixed radiation-convection boundary layer flow of an optically dense fluid along a vertical flat plate in a non-Darcy porous medium, *Int. J. Applied Mechanics Engineering*, **8**, pp. 483–496, 2003.
21. A. J. Chamkha, H. S. Takhar, O. A. Bég, Radiative free convective non-Newtonian fluid flow past a wedge embedded in a porous medium, *Int. J. Fluid Mechanics Research*, **31**, pp. 101–115, 2004.
22. A. Raptis, C. Perdikis, Unsteady flow through a highly porous medium in the presence of radiation, *Transport Porous Media J.*, **57**(2), pp. 171–179, 2004.
23. H. S. Takhar, A. J. Chamkha, R. S. R. Gorla, Combined convection-radiation interaction along a vertical flat plate in a porous medium, *Int. J. Fluid Mechanics Research*, **32**, pp. 139–156, 2005.
24. V. M. Soundalgekar, Free convection and mass transfer effects on the flow past an impulsively-started vertical plate, *ASME J. Applied Mechanics*, **46**, pp. 757–760, 1979.
25. K. Stewartson, On the impulsive motion of a flat plate in a viscous fluid, *Quart. J. Mechanics Applied Mathematics*, **4**, pp. 182–198, 1951.
26. R. Muthukumaraswamy, P. Ganesan, Unsteady flow past an impulsively-started vertical plate with heat and mass transfer, *Heat Mass Transfer J.*, **34**, pp. 187–193, 1998.
27. A. A. Raptis, A. K. Singh, Free convection flow past an impulsively started vertical plate in a porous medium by the finite difference method, *Astrophysics Space Science J.*, **112**, pp. 259–265, 1985.
28. P. Ganesan, P. Loganathan, V. M. Soundalgekar, Radiation effects on flow past an impulsively started plate, *Int. J. Applied Mechanics Engineering*, **6**(3), pp. 719–730, 2001.

29. D. Incropera, P. Dewitt, *Fundamentals of Heat and Mass Transfer*, MacGraw-Hill, 1993.
30. V. R. Prasad, N. B. Reddy, R. Muthucumaraswamy, Radiation and mass transfer effects on two-dimensional flow past an impulsively started infinite vertical plate, *Int. J. Thermal Sciences*, **46**(12), pp. 1251–125, 2007.
31. J. Zueco, Numerical study of an unsteady free convective magnetohydrodynamic flow of a dissipative fluid along a vertical plate subject to constant heat flux, *Int. J. Engineering Science*, **44**, pp. 1380–1393, 2006.
32. J. Zueco, F. Alhama, Simultaneous inverse determination of the temperature-dependent thermophysical properties of fluids using the network simulation method, *Int. J. Heat Mass Transfer*, **50**, pp. 3234–3243, 2007.
33. J. Zueco, A. Campo, Transient radiative transfer between the thick walls of an enclosure using the network simulation method, *Applied Thermal Engineering*, **26**, pp. 673–679, 2006.
34. J. Zueco, Network method to study the transient heat transfer problem in a vertical channel with viscous dissipation, *Int. Comm. Heat Mass Transfer*, **33**, pp. 1079–1087, 2006.
35. *Pspice 6.0*, Irvine, California 92718, Microsim Corporation, 20 Fairbanks, 1994.
36. R. Siegel, J.R. Howell, *Thermal Radiation Heat Transfer*, Student Edition, MacGraw-Hill, 1972.
37. H. Schlichting, *Boundary-Layer Theory*, 7th edition, MacGraw-Hill, 1979.